Full paper

Chinese knot-like electrode design for advanced Li-S batteries

Chunlong Dai[a,1], Linyu Hu[a,1], Xinyu Li[b], Qiuju Xu[a], Rui Wang[a], Heng Liu[a], Hao Chen[a], Shu-Juan Bao[a], Yuming Chen[c,*], Graeme Henkelman[b,*], Chang Ming Li[a], Maowen Xu[a,*]

[a] Faculty of Materials and Energy, Southwest University, Chongqing 400715, PR China
[b] Texas Materials Institute and Department of Chemistry and the Institute for Computational Engineering and Sciences, University of Texas at Austin, Austin, TX 78712, USA
[c] Department of Nuclear Science and Engineering, Department of Materials Science and Engineering, Massachusetts Institute of Technology, Cambridge, MA 02139, USA

ARTICLE INFO

ABSTRACT

Rational design of Li-S batteries requires efficient prevention of sulfur mobility and fast redox kinetics while accommodating the volumetric expansion of the sulfur cathode. Herein, we propose a multifunctional Chinese knot-like electrode design for advanced Li-S batteries. $NiCo_2S_4$ nanotubes are closely interwoven to form Chinese knot-like designs as a sulfur host. The unique interconnectivity of the 2D Chinese knot-like networks constructed by 1D nanostructured nanotubes enables fast electron transfer for high capacity. Furthermore, the hollow structure can simultaneously provide enough space for volumetric expansion of sulfur and confine lithium polysulfides (LiPSs) in the internal void space by structural encapsulation. Besides these, experimental and theoretical analysis demonstrates that $NiCo_2S_4$ can effectively capture the LiPSs and then catalyze the captured LiPSs into solid Li_2S_2/Li_2S. More importantly, the transition between low-spin and high-spin of Co ions, induced by extra sulfur atoms from LiPSs, provides an electronic way to stabilize the adsorption system and reduce system energy, leading to the inhibition of the shuttle effect in Li-S batteries. As a result, the Chinese knot-like S@$NiCo_2S_4$ electrodes show a high capacity of $1348\,\mathrm{mA\,h\,g^{-1}}$ at 0.1 C and long cycling life up to 1000 cycles with a slow capacity decay of 0.02% per cycle at 1 C. Even with a higher sulfur loading of $5\,\mathrm{mg\,cm^{-2}}$, the electrodes still deliver good electrochemical performance.

1. Introduction

Lithium-sulfur (Li-S) batteries have been spotlighted in view of their high energy density and abundant resources [1–3]. However, the practical application of Li-S batteries remains hindered by low utilization of sulfur and short cycle life [4,5] due to the poor conductivity of sulfur [6–8], the dissolution of intermediate lithium polysulfides (LiPSs) into the electrolyte, slow redox kinetics of LiPSs, and the severe volumetric expansion (~ 80%) during cycling [9–11]. To improve the electrochemical performance of Li-S batteries, extensive research efforts have been devoted to overcoming these challenges. In the early years, various carbonaceous materials have been studied as the sulfur host due to their high conductivity [12–18]. However, their nonpolar nature is not able to help efficiently trap the LiPSs [19].

Recently, polar materials including metal hydroxides [20,21], metal oxides [22–26], nitrides [27–30], and sulfides [31–37] have been demonstrated to strongly bind LiPSs. However, due to sluggish redox kinetics of LiPSs, it is difficult for the fixed LiPSs to fully convert to $Li_2S_2/$

Li_2S, resulting in low utilization of sulfur and low rate capability. More seriously, a mass of LiPSs will gather in the areas far away from the host materials. The high concentration of LiPSs is easy to dissolve in the electrolyte to diffuse onto lithium anode, and then react with lithium, thus resulting in severe shuttle effect. Recent studies have shown that some catalysts, such as Pt [38], CoS_2 [39], and TiC [40] can accelerate polysulfide redox kinetics. Therefore, the sulfur host materials need possess polar chemisorptive capability and the ability to facilitate the transformation between the soluble LiPSs and insoluble products simultaneously. Unfortunately, these solid host materials with the irregular morphology show some serious problems. For example, the shuttle effect is still severe when these electrodes with high sulfur loading because the irregular solid hosts are only able to confine and catalyze the LiPSs near their surface [41]. One feasible way is to design these host materials with some hollow nanostructures. Compared to solid counterpart, the hollow nanostructure has the following advantages: i) providing enough internal void space for high sulfur loading; ii) accommodating the volumetric expansion of sulfur; iii)

---

* Corresponding authors.
E-mail addresses: yumingc126@126.com, yumingc@mit.edu (Y. Chen), henkelman@utexas.edu (G. Henkelman), xumaowen@swu.edu.cn (M. Xu).
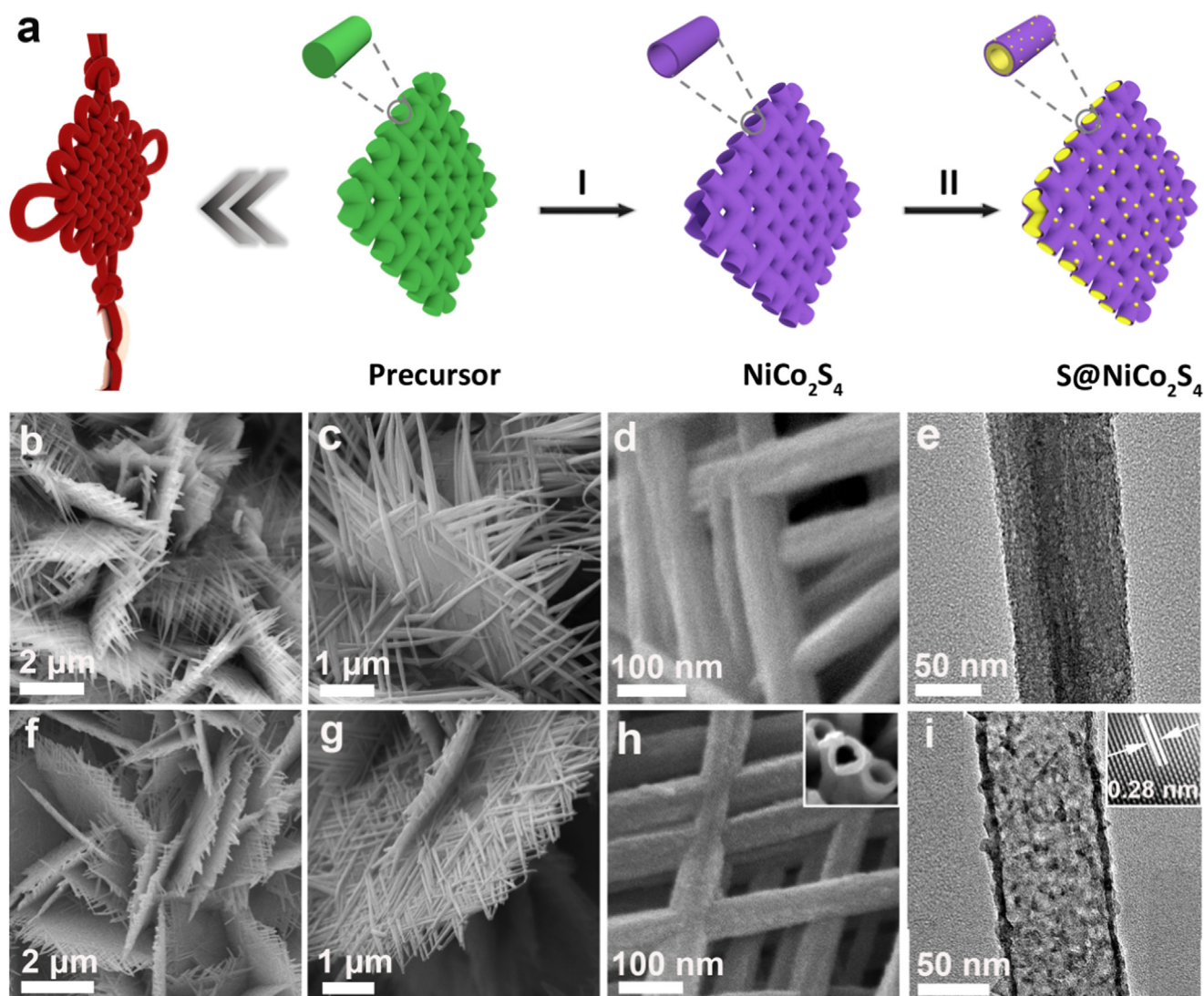[1] These authors contributed equally to this work.

Fig. 1. Schematic illustration of the Chinese knot-inspired electrode design and characterization of the prepared materials. (a) Illustration of the synthesis of the Chinese knot-like S@NiCo$_2$S$_4$ composites. (b-d) FESEM and (e) TEM images of the knot-like precursors. (f-h) FESEM and (i) TEM images of the knot-like NiCo$_2$S$_4$ matrixes.

exposing more adsorption and catalytic sites; iv) promising more efficient encapsulation of LiPSs by locking them in the internal void space. On the other hand, for the isolated nanoparticles, it is hard for electrons or lithium ions continuously transport among them, thus leading to considerable contact resistance. Moreover, the use of nanoparticles often leads to low packing density of the electrode. An effective method is to fabricate microstructured interconnected network constructed from secondary structure of nanomaterials. Based on the aforementioned discussion, an ideal sulfur host is expected to possess these merits: i) excellent electrical conductivity; ii) strong chemisorptive capability to LiPSs; iii) an ability to facilitate the conversion reaction of LiPSs; iv) hollow structure; and v) microstructured conductive network construct from secondary structure of nanomaterials.

Here we propose a multifunctional Chinese knot-like electrode design to fulfill aforementioned requirements. Hollow NiCo$_2$S$_4$ nanotubes are closely interwoven to form Chinese knot-like designs as the sulfur host. First, NiCo$_2$S$_4$ shows excellent electrical conductivity, ~ 100 times higher than that of NiCo$_2$O$_4$. Moreover, binary metal sulfide such as NiCo$_2$S$_4$ often exhibits higher electrochemical activity than mono-metal sulfides, including Co$_9$S$_8$, NiS and TiS$_2$ [42]. Second, NiCo$_2$S$_4$ can effectively fix the LiPSs due to the polar chemisorptive capability and catalyze the fixed LiPSs to Li$_2$S$_2$/Li$_2$S. Therefore, strong trapping and

fast LiPSs conversion can be realized in the NiCo$_2$S$_4$ nanotube simultaneously, thus eliminating the shuttle effect and improving sulfur utilization. Third, the internal void space of NiCo$_2$S$_4$ nanotube serves as a nanoscale electrochemical reaction vessel for immobilizing and catalyzing LiPSs. And the shell of nanotube acts as a gate to encapsulate the LiPSs in the hollow core. More importantly, these 1D hollow nanotubes are interconnected to form a 2D Chinese knot-like network that is beneficial to fast transfer of electrons and lithium ions. As a result, the Chinese knot-like S@NiCo$_2$S$_4$ electrode shows high capacity, good rate performance and excellent cycling stability.

2. Results and discussion

Inspired by the fascinating structure of Chinese knot and the conspicuous merits of hollow structured host materials, this work intends to combine the advantages of these two structures together to fabricate hollow Chinese knot-like designs as the sulfur host. The synthesis approach of Chinese knot-like S@NiCo$_2$S$_4$ electrode is schematically shown in Fig. 1a. First, the precursor, with a Chinese knot-like structure, was prepared by a facile hydrothermal method without any templates or surfactants. Second, the solid precursor was converted into hollow NiCo$_2$S$_4$ through a sulfidation reaction. Finally, a melting-
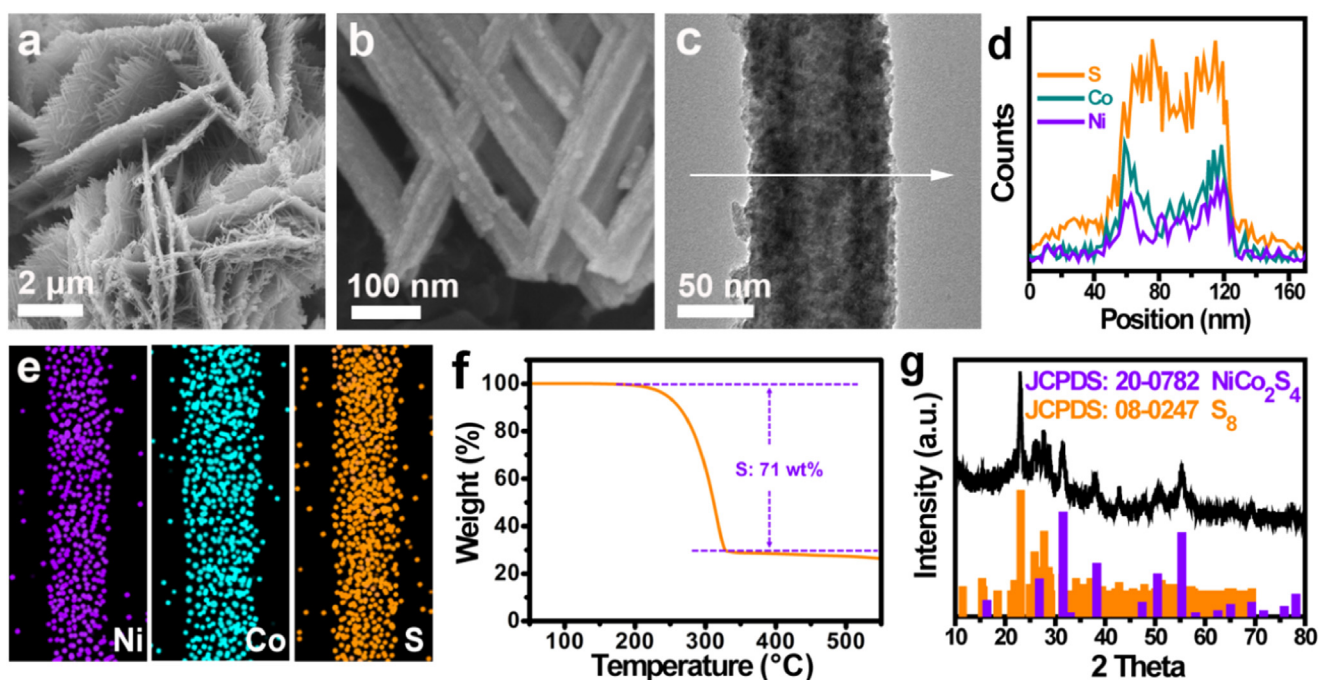
Fig. 2. Characterization of Chinese knot-like S@NiCo$_2$S$_4$ composite. (a, b) FESEM and (c) TEM images of the S@NiCo$_2$S$_4$. (d) Linear elemental distributions and (e) EDX elemental mappings of S, Co, and Ni. (f) TGA curve and (g) XRD pattern of the S@NiCo$_2$S$_4$ composite.

diffusion process was employed to steam sulfur into the NiCo$_2$S$_4$ nanotubes, enabling the Chinese knot-like S@NiCo$_2$S$_4$ composite.

The morphology of the precursor was characterized by field-emission scanning electron microscopy (FESEM) and transmission electron microscopy (TEM). After a hydrothermal treatment, the precursor displays a 2D structure which is interwoven by 1D solid nanorods (Fig. 1b-d). The diameter of the nanorod is estimated to be about 80 nm (Fig. 1e). The hydrothermal reaction time plays an important role in the formation of the unique Chinese knot-like structure (Figs. S1 and S2). After a sulfidation reaction, the XRD pattern of the product is perfectly assigned to NiCo$_2$S$_4$ (Fig. S3). The NiCo$_2$S$_4$ still maintains the Chinese knot-like morphology (Fig. 1f, g). Meanwhile, the solid nanorod can be turned into hollow tubular structure by an anion exchange reaction (Fig. 1h, i), thus perfectly combining the merits of interconnectivity of Chinese knot network and hollow structure. The low-magnification TEM images exhibits good uniformity of the hollow structure (Fig. S4). It is obvious that these 1D hollow nanotubes are interconnected, which is beneficial to fast transfer of electrons and lithium ions. It is worth mentioning that the shell of the nanotube is extraordinary thin, thus providing a considerable internal void space for abundant sulfur storage. HRTEM study shows a clear lattice spacing of 0.28 nm, corresponding to the (311) plane of NiCo$_2$S$_4$ (Fig. 1i). The specific surface area of the NiCo$_2$S$_4$ is about 36.2 m^2 g^{-1} (Fig. S5).

After the loading of sulfur, as shown in Fig. 2a, the S@NiCo$_2$S$_4$ well preserved the original Chinese knot-like morphology. It is clear that no obvious sulfur particles are observed on the outer surface (Fig. 2b). TEM image manifests that sulfur is uniformly and closely distributed in the internal void space of the NiCo$_2$S$_4$ nanotube (Fig. 2c), promising good electronic contact to the nanotube. Some unfilled spaces still exist in the nanotube, which can accommodate sulfur volume expansion during cycling. Fig. 2d shows linear elemental distributions across a typical S@NiCo$_2$S$_4$ nanotube, with much higher S intensity than that of initial NiCo$_2$S$_4$ nanotube (Fig. S6), suggesting successful introduction of sulfur into the inner void spaces of nanotube. EDX elemental mapping (Fig. 2e) of S@NiCo$_2$S$_4$ composite also reveals that sulfur is distributed in the hollow tubules of the NiCo$_2$S$_4$. Based on the TGA and DSC curves of the pure NiCo$_2$S$_4$ and S@NiCo$_2$S$_4$ composite, the content of sulfur calculated in the composite is ~ 71 wt% (Fig. 2f, S7, and S8) [43]. The

XRD pattern of the as-obtained composite indicates cubic sulfur (JCPDS No. 08-0247) and NiCo$_2$S$_4$ (Fig. 2g).

To identify the chemical interaction between NiCo$_2$S$_4$ and LiPSs, we employed a combination of visual discrimination and XPS analysis. As displayed in Fig. 3a, the color of the LiPSs solution remains yellow after adding the carbon black (CB). However, the yellow solution transforms to completely colorless after the addition of NiCo$_2$S$_4$ (Fig. 3b), revealing the strong LiPSs adsorption capability of the polar NiCo$_2$S$_4$. To further probe the LiPSs absorptivity of NiCo$_2$S$_4$, the XPS test was carried out to investigate the pristine NiCo$_2$S$_4$ and NiCo$_2$S$_4$ + Li$_2$S$_4$. After contact with Li$_2$S$_4$, the peaks of both the Ni 2p$_{3/2}$ and Co 2p$_{3/2}$ spectrum shift to lower binding energy as the electron transfers from Li$_2$S$_4$ to the Ni and Co atoms (Fig. 3c, d), demonstrating the strong chemical interaction between NiCo$_2$S$_4$ and the LiPSs.

To investigate the effect of NiCo$_2$S$_4$ on LiPSs redox reactions, the cyclic voltammetry (CV) and galvanostatical discharge-charge tests were performed. Fig. 3e shows the typical CV profiles of the S@NiCo$_2$S$_4$ and S@CB cathodes. Compared to the S@CB electrode, the peaks of S@NiCo$_2$S$_4$ electrode are sharper with a higher intensity, indicating that the redox reactions at these potentials are greatly promoted [44,45]. Figs. S9 and S10 show the comparison of the peak potentials and onset potentials of the two electrodes for the redox reactions, respectively. Both cathodic peaks for S@NiCo$_2$S$_4$ have a positive shift and the anodic peak has a negative shift, reflecting that NiCo$_2$S$_4$ can significantly suppress the electrochemical polarization [46,47]. Clearly, the S@NiCo$_2$S$_4$ electrode shows a higher onset reduction potential and a lower onset oxidation potential than that of S@CB cathodes, showing that NiCo$_2$S$_4$ plays an important role in reducing the activation energy of the transformation between LiPSs [48–50].

The galvanostatic discharge-charge profiles of S@CB and the S@NiCo$_2$S$_4$ electrodes at 0.1 C are shown in Fig. 3f. The higher capacity, longer voltage plateau, and lower polarization of the NiCo$_2$S$_4$-based electrode suggest that NiCo$_2$S$_4$ can serve as a good catalyst to realize highly reversible redox process and improve the utilization of active materials [51]. There is no obvious peak in the CV curve of pure NiCo$_2$S$_4$ electrodes (Fig. S11). Additional evidence on the catalytic effect of NiCo$_2$S$_4$ was provided by CV and electrochemical impedance spectra (EIS) of symmetric cells. Fig. S12 shows the CV profiles of the
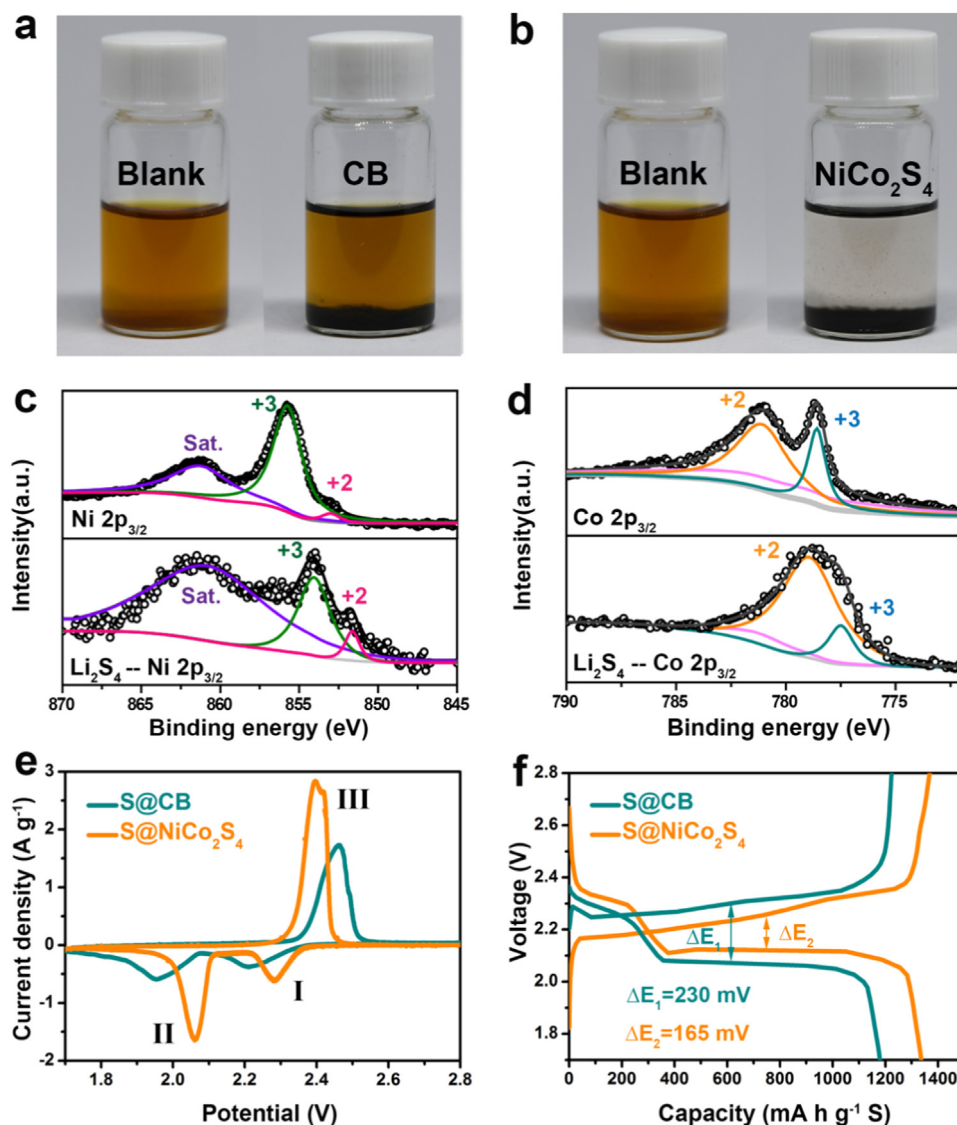
Fig. 3. NiCo$_2$S$_4$ adsorbs LiPSs and promotes electrochemical reaction kinetics of LiPSs. Polysulfide entrapment by (a) carbon black and (b) NiCo$_2$S$_4$. The comparison of high-resolution XPS spectra of Ni 2p$_{3/2}$ (c) and Co 2p$_{3/2}$ (d) of the pure NiCo$_2$S$_4$ and NiCo$_2$S$_4$ + Li$_2$S$_4$ composite. The comparison of (e) CV curves and (f) discharge-charge curves of S@NiCo$_2$S$_4$ and S@CB electrodes.

symmetric cells within a voltage window of − 0.8 to 0.8 V at a scan rate of 20 mV s^{-1}. The redox current of the NiCo$_2$S$_4$ electrode is much larger than that of pure CB electrode. Meanwhile, the EIS of NiCo$_2$S$_4$ electrode shows a decrease of about 71% in resistance compared to pure CB electrode (Fig. S13), which is similar to other literatures [35,39,40]. These results indicate that NiCo$_2$S$_4$ can dynamically promote the electrochemical reactions between LiPSs.

The electrochemical performance of the sulfur loading of ∼ 2 mg cm^{-2} was evaluated. The thickness of the electrode is about 30 μm (Fig. S14). As shown in Fig. 4a, the Chinese knot-like S@NiCo$_2$S$_4$ electrode exhibits excellent rate capability under various current rates. The cathode delivers reversible discharge capacities of 1348, 1227, 1050, 926 and 842 mA h g^{-1} at different rates of 0.1, 0.2, 0.5, 1 and 2 C, respectively. In contrast, the S@CB electrode shows much lower discharge capacities. Fig. 4b presents the discharge-charge voltage profiles of the electrode at various current densities from 0.1 to 2 C. The discharge-charge voltage profiles at 2 C are similar to that at 0.1 C, showing long second-discharge plateau and a small polarization. The long-term cycling performance of S@NiCo$_2$S$_4$ electrode was evaluated by galvanostatic cycling at 1 C (Fig. 4c). The initial discharge specific capacity of S@NiCo$_2$S$_4$ electrode is about 932 mA h g^{-1} and a discharge

capacity of 741 mA h g^{-1} maintains after 1000 cycles, corresponding to only 0.02% average capacity decay per cycle, lower than that of most other polar hosts (Fig. S15). By sharp contrast, the S@CB electrode fades quickly. In addition, the self-discharge behavior of S@NiCo$_2$S$_4$ cell is alleviated (Fig. S16). It is worth mentioning that pure NiCo$_2$S$_4$ shows almost no contribution to capacity under the same conditions (Fig. S17). In order to further reveal the merits of Chinese knot-like network, we prepared flower-like NiCo$_2$S$_4$ as the host of sulfur for comparison. The flower-like S@NiCo$_2$S$_4$ composites suffer from faster capacity decay and delivers lower capacities at 0.1, 0.2, 0.5, 1, and 2 C when compared to that of the Chinese knot-like S@NiCo$_2$S$_4$ composite (Figs. S18 and S19). These results demonstrated the unique advantages of Chinese knot-like morphology.

The development of high areal sulfur loading is vital to the commercial application of Li-S batteries. Herein, we further studied the electrochemical performance of S@NiCo$_2$S$_4$ electrode with a high loading of 5 mg cm^{-2}, which is higher than most other polar host materials (Fig. S20). The cross section of the high loading electrode is shown in Fig. S21. The As shown in Fig. 4d **and** S22, the thick S@NiCo$_2$S$_4$ electrode delivers reversible discharge capacities of about 1180 (5.9 mAh cm^{-2}), 970 (4.85 mAh cm^{-2}), 840 (4.2 mAh cm^{-2}), and
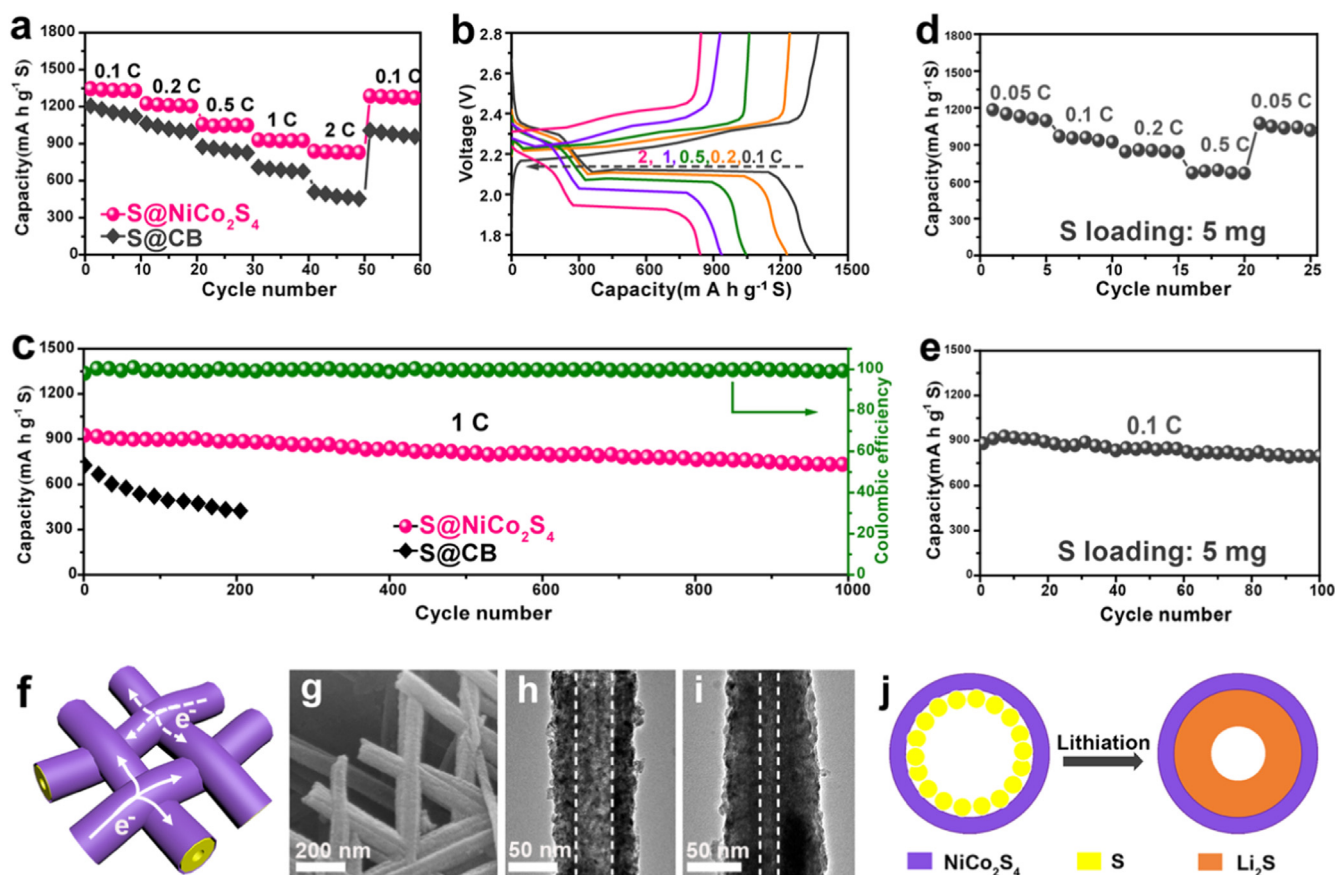
Fig. 4. Electrochemical performances of the Chinese knot-like S@NiCo$_2$S$_4$ electrodes. (a) Rate capabilities, (b) discharge-charge curves, and (c) cycling performance of Chinese knot-like S@NiCo$_2$S$_4$ electrodes with a sulfur loading of 2 mg cm^{-2}. (d) Rate capabilities and (e) cycling performance of the designs with high sulfur loading of 5 mg cm^{-2}. (f) Schematic of the structural advantages of Chinese knot-like cathode designs. (g) FESEM images of the S@NiCo$_2$S$_4$ composite after cycling. TEM images of the S@NiCo$_2$S$_4$ composite at fully (h) charged and (i) discharged state. (j) Schematic of NiCo$_2$S$_4$ nanotube relieving the volumetric expansion of sulfur during lithiation process.

700 mAh g^{-1} (3.5 mAh cm^{-2}) at different rates of 0.05 C, 0.1 C, 0.2 C, and 0.5 C, respectively. Moreover, the thick electrode also shows stable cycling performance. The electrode displays an initial capacity of about 890 mAh g^{-1} (4.45 mAh cm^{-2}) at 0.1 C and increases to 945 mAh g^{-1} at the 7th cycle due to the activate process. A high capacity of about 810 mAh g^{-1} (4.05 mAh cm^{-2}) after 100 cycles can still be achieved, corresponding to only 0.14% average capacity decay per cycle (Fig. 4e and S23).

In order to explore the structural stability of the NiCo$_2$S$_4$ network, we studied the morphology of the S@NiCo$_2$S$_4$ composite after cycling. As shown in Fig. 4g, the Chinese knot-like interconnected structure is well preserved after long-term cycling, demonstrating the outstanding structural stability. To further investigate whether the hollow tubular structure effectively accommodate the volumetric expansion of sulfur after lithiation, we tested the NiCo$_2$S$_4$ nanotubes at fully charged and discharged state after cycling. As shown in Fig. 4h, i, both the size and shape of the nanotube can be well maintained. There still exists some void spaces in the nanotube at fully discharged state, indicating that NiCo$_2$S$_4$ nanotube offers sufficient room to accommodate the volume expansion of sulfur during lithiation process (Fig. 4j). The internal void space of NiCo$_2$S$_4$ nanotube at fully discharged state is much smaller than that at fully charged state, which is attributed to the volumetric expansion of sulfur changed into Li$_2$S$_2$/Li$_2$S. The linear elemental distribution of the discharged nanotubes (Fig. S24) shows that the sulfur signal in the middle of the nanotube is enhanced as compared with that of initial S@NiCo$_2$S$_4$ (Fig. 2d), further proving the volumetric expansion of sulfur. The calculated volume expansion based on Fig. 4h and i (71%) is a little smaller than the theoretical value (80%). This is

because some sulfur materials are on the outer surface of the nanotubes and some are in the pores of NiCo$_2$S$_4$ (See Supplementary note). These observations reveal that NiCo$_2$S$_4$ can act as a robust host with the excellent electrochemical performance.

We further studied the lithium-metal anodes after 50 cycles by FESEM and EDX analysis. As shown in Fig. S25, no obvious lithium dendrite is observed on the lithium surface for the S@NiCo$_2$S$_4$ cell. Meanwhile, the signal of sulfur on the lithium anode is negligible. However, the lithium anode in the S@CB cell suffers serious damage and its surface is corroded into tiny particles. Moreover, the signal of sulfur on the lithium anode caused by shuttled polysulfide is much stronger than that of S@NiCo$_2$S$_4$ cell. The S to O ratio on lithium surface from S@NiCo$_2$S$_4$ is also much smaller than that of S@CB cells (Table S1). These results indicate that the multifunctional hierarchical electrode can suppress shuttle effect effectively.

We simulated the adsorption processes of LiPSs on several surfaces of NiCo$_2$S$_4$ to further study the chemical interaction between NiCo$_2$S$_4$ and LiPSs. (400) and (440) surfaces were discovered as stable surfaces and used for further adsorption calculations, shown in Fig. 5a. Surface reconstruction has been discovered on several surfaces. For example, sulfur atoms tend to form small sulfur clusters on some sulfur-rich surfaces during surface structural relaxations. In our calculation, we found that all Li$_2$S$_4$, Li$_2$S$_6$ and Li$_2$S$_8$ particles can be adsorbed at multiple sites on both (400) and (440) surfaces. The spin-polarized simulation shows that surface Co ions around adsorption site will experience a transition between low-spin and high-spin states. On clean NiCo$_2$S$_4$ surfaces, Co ions are in low-spin states. When LiPS particles are adsorbed on surfaces, one or several Co ions around LiPSs transit to high-

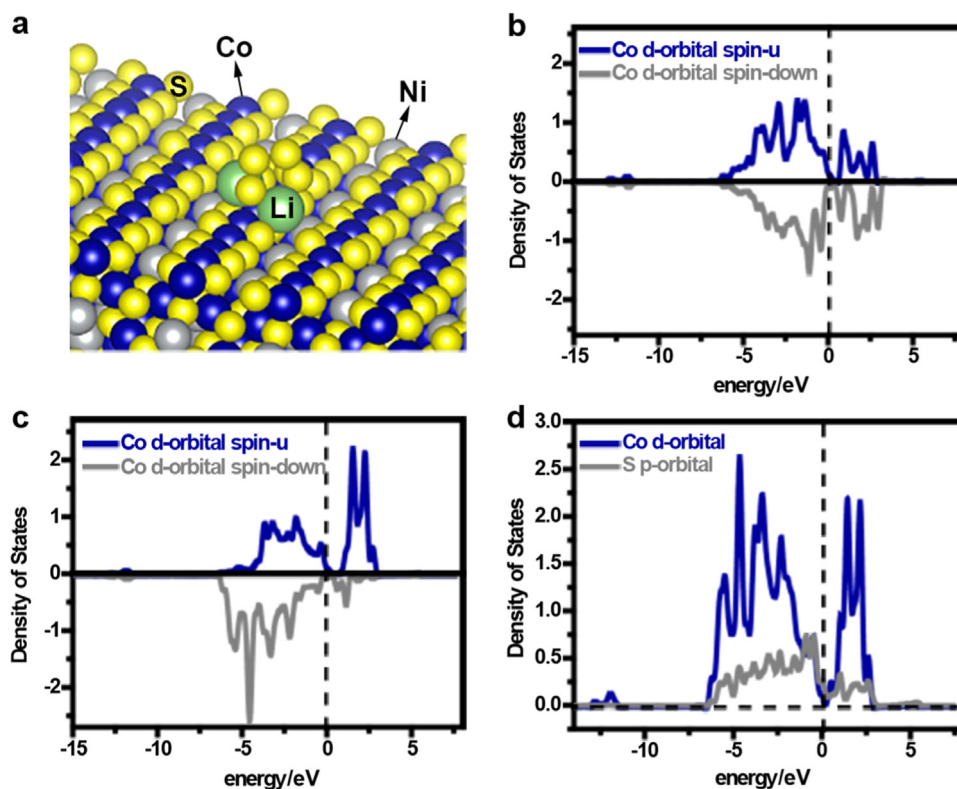**Fig. 5.** Theoretical calculations. (a) A Li_2S_6 particle adsorbed on (440) surface of $NiCo_2S_4$. (b) Low-spin and (c) high-spin states of Co d-orbital in low-spin to high-spin transition. (d) Density of states of Co d-orbital and S p-orbital. The Co ion is on (440) surface close to adsorption site and the S comes from Li_2S_6 particle.

spin states, number of high-spin Co ions depends on the adsorption site and configuration of LiPSs particles. Density of states of low-spin and high-spin d-orbitals are plotted in Fig. 5b, c. Density of states of Co's d-orbital and S's p-orbital are shown in Fig. 5d. Electronic configuration of Ni ion is relatively stable during the adsorption of LiPSs. The charge state change on Ni has been observed on Ni in some cases. It is possible that Ni has spin or charge state change to tolerate the LiPSx particles. Our simulation shows that, other than structural change, the transition between low-spin and high-spin of Co ions, induced by extra sulfur atoms from LiPSs, provides an electronic way to stabilize the adsorption system and reduce system energy, alleviating the shuttle effect in Li-S batteries.

The Chinese knot-like electrode design provides many advantages for Li-S batteries. First, for the conventional isolated host materials, as shown in Fig. S26, it is hard for electrons or lithium ions continuously conduct among them on account of the considerable contact resistance. However, for the Chinese knot-like structure, both the 1D substructures and the interconnectivity of the 2D network are beneficial for fast electron transfer (Fig. 4f). Second, the interwoven network possesses good mechanical strength to maintain the structural integrity, thus enabling excellent cycling performance. Third, the micrometer-sized network constructed from nanotubes can avoid the low packing density of nanoparticles. Fourth, hollow structure provides numerous anchoring and catalyzing sites for the polysulfide intermediates. Moreover, the internal void space can promise abundant sulfur storage and act as an ideal reaction vessel for immobilizing and catalyzing LiPSs. Finally, the relatively large surface area provided by the hollow structure guarantees uniform deposition of Li_2S_2/Li_2S.

3. Conclusions

In summary, we have designed and fabricated Chinese knot-like electrode designs for Li-S batteries. This interpenetrating hollow structure is beneficial for providing continuous electron transfer,

maintaining the structural integrity, and suppressing LiPSs outward diffusion simultaneously. Experiment and simulation demonstrate that $NiCo_2S_4$ can serve as a polysulfide immobilizer and catalyst simultaneously in Li-S batteries. Benefiting from the compositional and structural superiorities, the Chinese knot-like S@$NiCo_2S_4$ composite cathode with a high sulfur loading of $5\ mg\ cm^{-2}$ delivers a stable cycle life with a high discharge capacity.

Appendix A. Supporting information

Supplementary data associated with this article can be found in the online version at doi:10.1016/j.nanoen.2018.08.065.

References

[1] A. Manthiram, Y. Fu, S.-H. Chung, C. Zu, Y.-S. Su, Chem. Rev. 114 (2014) 11751–11787.
[2] Q. Pang, X. Liang, C.Y. Kwok, L.F. Nazar, Nat. Energy 1 (2016) 16132.
[3] J. Lu, T. Wu, K. Amine, Nat. Energy 2 (2017) 17011.
[4] Z.W. Seh, Y. Sun, Q. Zhang, Y. Cui, Chem. Soc. Rev. 45 (2016) 5605.
[5] R. Xu, J. Lu, K. Amine, Adv. Energy Mater. 5 (2015) 1500408.
[6] H.-J. Peng, J.-Q. Huang, X.-B. Cheng, Q. Zhang, Adv. Energy Mater. 7 (2017) 1700260.
[7] S. Xin, L. Gu, N.H. Zhao, Y.X. Yin, L.J. Zhou, Y.G. Guo, L.J. Wan, J. Am. Chem. Soc. 45 (2012) 18510–18513.
[8] R. Fang, S. Zhao, Z. Sun, D.W. Wang, H.M. Cheng, F. Li, Adv. Mater. 48 (2017) 1606823.
[9] Z. Cui, C. Zu, W. Zhou, A. Manthiram, J.B. Goodenough, Adv. Mater. 28 (2016)

6926–6931.

[10] S. Rehman, K. Khan, Y. Zhao, Y. Hou, J. Mater. Chem. A 5 (2017) 3014.
[11] X. Liu, N. Xu, T. Qian, J. Liu, X. Shen, C. Yan, Nano Energy 41 (2017) 758–764.
[12] F. Wu, J. Qian, R. Chen, T. Zhao, R. Xu, Y. Ye, W. Li, L. Li, J. Lu, K. Amine, Nano Energy 12 (2015) 742–749.
[13] X.X. Peng, Y.Q. Lu, L.L. Zhou, T. Sheng, S.Y. Shen, H.G. Liao, L. Huang, J.T. Li, S.G. Sun, Nano Energy 32 (2017) 503–510.
[14] P.Y. Zhai, H.J. Peng, X.B. Cheng, L. Zhu, J.Q. Huang, W.C. Zhu, Q. Zhang, Energy Storage Mater. 7 (2017) 56.
[15] Z. Chang, H. Dou, B. Ding, J. Wang, Y. Wang, G. Xu, C. Li, New J. Chem. 40 (2016) 7680.
[16] S.Y. Lu, M. Jin, Y. Zhang, Y.-B. Niu, J.C. Gao, C.M. Li, Adv. Energy Mater. (2017) 1702545.
[17] F. Pei, L. Lin, D. Ou, Z. Zheng, S. Mo, X. Fang, N. Zheng, Nat. Commun. 8 (2017) 482.
[18] Z. Chang, B. Ding, H. Dou, J. Wang, G. Xu, X. Zhang, Chem. -Eur. J. 24 (2018) 3768.
[19] K. Mi, S. Chen, B. Xi, S. Kai, Y. Jiang, J. Feng, Y. Qian, S. Xiong, Adv. Funct. Mater. 27 (2017) 1604265.
[20] J. Jiang, J. Zhu, W. Ai, X. Wang, Y. Wang, C. Zou, W. Huang, T. Yu, Nat. Commun. 6 (2015) 8622.
[21] C. Dai, L. Hu, Q. Wang, Y. Chen, J. Han, J. Jiang, Y. Zhang, B. Shen, Y. Niu, S. Bao, M. Xu, Energy Storage Mater. 8 (2017) 202.
[22] Z.W. Seh, W.Y. Li, J.J. Cha, G.Y. Zheng, Y. Yang, M.T. McDowell, P.C. Hsu, Y. Cui, Nat. Commun. 4 (2013) 1331.
[23] Z. Li, J. Zhang, X.W. Lou, Angew. Chem. Int. Ed. 54 (2015) 12886.
[24] L. Hu, C. Dai, H. Liu, Y. Li, B. Shen, Y. Chen, S.-J. Bao, M. Xu, Adv. Energy Mater. (2018) 1800709.
[25] J. He, L. Luo, Y. Chen, A. Manthiram, Adv. Mater. 29 (2017) 1702707.
[26] T. Chen, L. Ma, B. Cheng, R. Chen, Y. Hu, G. Zhu, Y. Wang, J. Liang, Z. Tie, J. Liu, Z. Jin, Nano Energy 38 (2017) 239–248.
[27] D.R. Deng, T.H. An, Y.J. Li, Q.H. Wu, M.S. Zheng, Q.F. Dong, J. Mater. Chem. A 4 (2016) 16184.
[28] N. Mosavati, S.O. Salley, K.Y.S. Ng, J. Power Sources 340 (2017) 210.
[29] D.R. Deng, F. Xue, Y.J. Jia, J.C. Ye, C.D. Bai, M.S. Zheng, Q.F. Dong, ACS Nano 11 (2017) 6031.
[30] T.G. Jeong, D.S. Choi, H. Song, J. Choi, S.A. Park, S.H. Oh, H. Kim, Y. Jung, Y.T. Kim, ACS Energy Lett. 2 (2017) 327–333.
[31] Q. Pang, D. Kundu, L.F. Nazar, Mater. Horiz. 3 (2016) 130.
[32] L. Hu, C. Dai, J.-M. Lim, Y. Chen, X. Lian, M. Wang, Y. Li, P. Xiao, G. Henkelman, M. Xu, Chem. Sci. 9 (2018) 666.
[33] H. Xu, A. Manthiram, Nano Energy 33 (2017) 124.
[34] C. Dai, J.-M. Lim, M. Wang, L. Hu, Y. Chen, Z. Chen, H. Chen, S. Bao, B. Shen, Y. Li, G. Henkelman, M. Xu, Adv. Funct. Mater. 28 (2018) 1704443.
[35] J. Pu, Z. Shen, J. Zheng, W. Wu, C. Zhu, Q. Zhou, H. Zhang, F. Pan, Nano Energy 37 (2017) 7.
[36] T. Chen, Z. Zhang, B. Cheng, R. Chen, Y. Hu, L. Ma, G. Zhu, J. Liu, Z. Jin, J. Am. Chem. Soc. 139 (2017) 12710.
[37] C. Ye, L. Zhang, C. Guo, D. Li, A. Vasileff, H. Wang, S.Z. Qiao, Adv. Funct. Mater. 27 (2017) 1702524.
[38] H. Al Salem, G. Babu, C.V. Rao, L.M. Arava, J. Am. Chem. Soc. 137 (2015) 11542.
[39] Z. Yuan, H.J. Peng, T.Z. Hou, J.Q. Huang, C.M. Chen, D.W. Wang, X.B. Cheng, F. Wei, Q. Zhang, Nano Lett. 16 (2016) 519.
[40] H.J. Peng, G. Zhang, X. Chen, Z.W. Zhang, W.T. Xu, J.Q. Huang, Q. Zhang, Angew. Chem., Int. Ed. 128 (2016) 13184.
[41] Z. Li, H.B. Wu, X.W. Lou, Energy Environ. Sci. 9 (2016) 3061.
[42] L.F. Shen, J. Wang, G.Y. Xu, H.S. Li, H. Dou, X.G. Zhang, Adv. Energy Mater. 5 (2015) 1400977.
[43] J. Yang, X. Duan, W. Guo, D. Li, H. Zhang, W. Zheng, Nano Energy 5 (2014) 74.
[44] H.J. Peng, J.Q. Huang, X.Y. Liu, X.B. Cheng, W.T. Xu, C.Z. Zhao, F. Wei, Q. Zhang, J. Am. Chem. Soc. 139 (2017) 8458.
[45] Z. Chang, H. Dou, B. Ding, J. Wang, Y. Wang, X. Hao, D.R. MacFarlane, J. Mater. Chem. A 5 (2017) 250.
[46] B.C. Yu, J.W. Jung, K. Park, J.B. Goodenough, Energy Environ. Sci. 10 (2017) 86.
[47] L. Li, L. Chen, S. Mukherjee, J. Gao, H. Sun, Z. Liu, X. Ma, T. Gupta, C.V. Singh, W. Ren, H.-M. Cheng, N. Koratkar, Adv. Mater. 29 (2017) 1602734.
[48] Y. Peng, B. Li, Y. Wang, X. He, J. Huang, J. Zhao, ACS Appl. Mater. Interfaces 9 (2016) 4397.
[49] C. Zheng, S. Niu, W. Lv, G. Zhou, J. Li, S. Fan, Y. Deng, Z. Pan, B. Li, F. Kang, Q.H. Yang, Nano Energy 33 (2017) 306.
[50] T. Zhou, W. Lv, J. Li, G. Zhou, Y. Zhao, S. Fan, B. Liu, B. Li, F. Kang, Q.H. Yang, Energy Environ. Sci. 10 (2017) 1694.
[51] G. Zhou, H. Tian, Y. Jin, X. Tao, B. Liu, R. Zhang, Z.W. Seh, D. Zhuo, Y. Liu, J. Sun, J. Zhao, C. Zu, D.S. Wu, Q. Zhang, Y. Cui, Proc. Natl. Acad. Sci. USA 114 (2017) 840.

Chunlong Dai received his M.S. degree under the guidance of Prof. Maowen Xu from Southwest University in June 2018. He is now pursuing his Ph.D. degree under the supervision of Prof. Liangti Qu at Beijing Institute of Technology (BIT). His research interests include the design and development of nanomaterials, and their application for energy conversion and storage devices.

Linyu Hu received her master's degree in Clear Energy Science from Southwest University under the guidance of Prof. Maowen Xu in June 2018. She is currently a Ph.D candidate at the School of Chemistry and Chemical Engineering at Beijing Institute of Technology (BIT) under supervision of Prof. Bo Wang. Her research interests focus on the design and synthesize novel nanomaterials and their applications in energy storage (Li-S batteries , Li/Na-ion batteries).

Xinyu Li is currently a Ph.D. candidate in materials science and engineering at the University of Texas at Austin, advised by Professor Graeme Henkelman and Professor Jianshi Zhou. He received his M.S. degree is materials science and engineering at Northwestern University in 2012. He received his B.E. degree in materials engineering at University of Science and Technology Beijing in 2010.

Qiuju Xu received her B.S. degree from Shandong Normal University in 2016. She is now pursuing his M.S. degree under the supervision of Prof. Maowen Xu at Southwest University. Her current research focuses on the design and synthesis of MOFs-based electrode materials for rechargeable batteries.
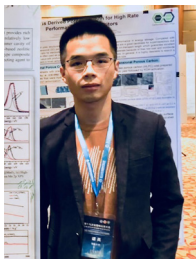

Rui Wang received his M.S. degree under the guidance of Associate Prof. Linna Zhu from Southwest University in June 2018. He is now working at Beijing Xinkaiyuan Pharmaceutical Technology Co., Ltd. His research interests include the design and development of organic materials, and their application for pharmaceuticals as well as organic optoelectronic devices.

Heng Liu is pursuing his M.S. degree under the guidance of Prof. Shujuan Bao at Southwest University. His research interest is focused on the design and fabrication of non-precious metal materials for energy conversion.

Graeme Henkelman is a professor of Chemistry and the Director of the Center for Computational Molecular Sciences in the Institute for Computational Engineering and Sciences at the University of Texas at Austin. He graduated with a degree in Physics from Queen's University in Canada, and a Ph.D. in Chemistry from the University of Washington. The Henkelman research group focuses on computational method for modeling reaction dynamics in chemical and material systems with a focus on energy applications.

Hao Chen is now pursuing his ph.D. degree under the guidance of Prof. Shujuan Bao at Southwest University. His main research field is nanomaterials and their application for fast energy storage.

Chang Ming Li is the Professor, Director of Institute of Clean Energy and Advanced Materials, Southwest University, Chongqing, China. He worked with Motorola as a distinguished technical member and Science Advisory Board Associate, and later became Professor, Head of Bioengineering Division and Director of Center for Advanced Bionanosystems in Nanyang Technological University, Singapore. He is Fellow of American institute of Medicine and Biological Engineering and RSC Fellow, serving as an Editorial Board Member of RSC advances and a member of Advisory Board for Nanoscales and Joule.

Shu-Juan Bao received her M.Sc. and Ph.D. in Materials Science from Xinjiang University and Lanzhou University (China) in 2003 and 2006. After completing a post-doctoral fellowship at Nanyang Technological University, she is currently a professor at Southwest University, China. Her research interests include controllable synthesis and functionalization of nanomaterials, and their important applications in nanoelectronics, biomedical devices and energy systems such as fuel cell, battery and supercapacitor.

Maowen Xu is currently a professor at the Faculty of Materials and Energy, Southwest University. He earned his Ph.D. degree from Lanzhou University. He worked as a postdoctoral scholar in Prof. J.B Goodenough's group of the University of Texas at Austin. He has published over 130 peer-reviewed journal papers with h-index of 28. His current research is focused on design and synthesis of electrode materials for sodium ion battery, lithium/sodium sulfur battery.

Yuming Chen received his Ph.D. degree from The Hong Kong Polytechnic University in 2014. He is now working as a postdoctoral follow in Prof. Ju Li's group in MIT. His current research interests include *in situ* TEM, energy storage, and energy harvesting.